Gold nanoparticles as absolute nano-thermometers

Journal:	*Nano Letters*
Manuscript ID	Draft
Manuscript Type:	Communication
Date Submitted by the Author:	n/a
Complete List of Authors:	Carattino, Aquiles; Leiden University, LION, Huygens-Kamerlingh Onnes Lab Caldarola, Martín; Leiden University, LION Orrit, Michel; Leiden University, LION

Gold nanoparticles as absolute nano-thermometers

Aquiles Carattino, Martín Caldarola, and Michel Orrit *

Huygens-Kamerlingh Onnes Lab, 2300RA Leiden, The Netherlands

E-mail: orrit@physics.leidenuniv.nl

Abstract

Nano-thermometry is a challenging field that can open the door to intriguing questions ranging from biology and medicine to material sciences. Gold nanorods are excellent candidates to act as nanoprobes because they are reasonably bright emitters upon excitation with a monochromatic source. Gold nanoparticles are commonly used in photothermal therapy as efficient transducers of electromagnetic radiation into heat. In this work we show that the spectrum of the anti-Stokes emission from gold nanorods irradiated in resonance can be used to measure the *absolute temperature* of the nanoparticles *without* the need of a previous calibration. The procedure can be easily implemented in any microscope capable of acquiring emission spectra.

Keywords

Gold nanorods, Plasmon, Anti-Stokes, Sensing, Temperature

Most physical, chemical and biological processes depend on temperature. Together with the miniaturization of devices and the advent of nanotechnology the need for measuring temperature with high spatial accuracy started to emerge. Notably in biology [1,2] and medicine [3]

measuring and controlling temperature at a sub-cellular scale will provide not only insight into intracellular processes but it will also contribute to a better understanding of the mechanisms involved in proposed new therapies such as photothermal tumor ablation [4] or controlled drug delivery.[5,6]

Nanometer-size probes with distinctive spectral features are ideal candidates for temperature measurements since they provide high spatial accuracy while far-field optics allow a non-contact readout. Some of the proposed strategies include structures that undergo a conformational change upon an increase in temperature,[7] thus inducing variations in fluorescence intensity of a dye molecule embedded into them.

Also cleverly designed lanthanide-based fluorescent probes in which the ratio of particular emission peaks depends on temperature allow a high accuracy and can be used as nanothermometers[8] even in biological samples.[9] Photobleaching is often an important limitation of these approaches. Recently, Surface Enhanced Raman Spectroscopy (SERS) allowed to measure spectral changes induced by temperature down to single molecules,[10] but a careful calibration of the measurements is crucial.

Gold nanoparticles continue to receive a fair amount of attention because of their unique optical properties.[11] The collective oscillation of conduction electrons, also known as plasmon, shows a resonance in the visible to near infra-red wavelengths. This resonance can be tuned by changing the shape of the particles[12] and is responsible for a large absorption and scattering cross section at the resonance wavelength. These cross sections can be calculated by solving the Maxwell equations numerically employing different computer packages,[13–15] obtaining a good agreement between calculations and what is experimentally achievable.

Thanks to the high absorption and scattering cross section (several times higher than the geometrical cross section) it is relatively simple to detect nanoparticles in a dark-field scattering configuration[16] or via photothermal imaging.[17,18] Alternatively, detecting gold nanoparticles through their luminescence[19] is also possible; their low quantum yield,[20–23] in the order of 10^{-5}, is compensated by the enhanced cross section at the surface plasmon

resonance (SPR). The luminescence signal is stable over time; gold nanoparticles do not blink nor bleach, therefore are useful labeling agents for processes that require extended periods of observation.[24]

Different metallic nano-objects are being introduced as agents for photothermal therapy[5,25] or drug delivery.[26] One of the advantages of gold nanoparticles is the possibility of tuning their resonance to the near infra-red range, where the penetration of light into tissues can be of several centimeters.[3–5,25,27,28] Moreover the particles can be used not only for treatment, but also for imaging.[5,29] In the case of photothermal therapy, nanoparticles are used as heat sources[4,27] to locally increase the temperature in order to induce the death of specific cells in a tissue.[5,25] However, the temperatures reached[30] can only be estimated from models[29] or from an ad-hoc calibration. Therefore a method that allows simultaneously to increase and to monitor the local temperature will be of great interest in a broad range of fields. In this paper we show that the anti-Stokes luminescence of gold nanorods can be used to measure their temperature with relatively high accuracy and without the need for previous calibration.

Luminescence of metallic nanoparticles has been the subject of extensive study in recent years. Since the first observation of luminescence from bulk gold,[31] different groups have tried to quantitatively describe the observed properties,[32,33] such as the quantum yield[20–23,34] and the emission spectrum.[35] In particular, gold nanorods present two distinct resonance energies, namely the transverse and the longitudinal plasmon resonances. These particles can therefore be excited efficiently at one of those energies; the transverse resonance corresponds to a wavelength of about 532 nm and will give rise to a broad luminescence emission with a peak at the longitudinal plasmon energy. Conversely it is possible to excite the particles with a wavelength matching the longitudinal plasmon resonance. In this case the excitation benefits from an enhanced absorption cross section, but the emission that overlaps the plasmon resonance will be mostly blocked by the filters needed to prevent direct excitation light from reaching the detectors.

In this work luminescence refers to the emission from nanoparticles observed at energies different from the excitation energy. Normally it is expected that after absorption of a photon, the electrons in the particle will relax and the emitted photons will appear at lower energies than the excitation. If this is the case, the emission is called Stokes-shifted; however gold nanoparticles when excited in resonance also present a significant emission at higher energies called anti-Stokes emission.[36–38]

The mechanism we propose to explain the luminescence from gold nanoparticles is based on the radiative recombination of electrons and holes that are created upon the absorption of an incident photon.[31,34] The emission will be enhanced by the presence of the surface plasmon acting as an antenna.[32] At the same time, the interaction of the electron or hole with a thermal bath (a phonon or another charge carrier) before recombining can give rise to an emitted photon with a higher energy than the excitation photon's.[39–41] This effect gives rise to secondary light emission, but can also be interpreted in part as a Raman scattering process.[42]

A monochromatic photon with energy $\hbar\omega_{\mathrm{L}}$ incident on the particle will give rise to a collective oscillation of the gas of conduction electrons called plasmon. The lifetime of the oscillation can be measured in pulsed experiments or estimated from the inverse of the linewidth and is in the order of 10 fs[43] (neglecting any dephasing time T_2^*). The plasmon decays by forming a pair of hot electron and hole with an internal energy equal to the plasmon energy.[44–46]

The hot electron and hole cool down by exchanging energy with the lattice on a timescale of $\tau \approx 1$ ps.[47] Before this happens, electron and hole have a small probability of recombining radiatively, i.e. of re-emitting their high electronic energy as a photoluminescence photon. If they have interacted only with static surfaces, their energy will be the same and therefore the emitted photon will have the same energy as the incoming photon, and will not contribute to the measured photoluminescence (as it will be blocked by the notch filter.) If, on the other hand, they have interacted with a phonon or a thermally excited electron or hole, they may

have lost or acquired energy before recombining.

Electron and hole can interact with baths before or upon recombination, either by creation or annihilation of phonons or interact with thermally excited charge carriers. In both cases the energy available upon recombination cannot much exceed $\hbar\omega_L + k_B T$. It has to be noted that in the hypothesis of a single-photon absorption at low excitation power, the temperature T is that of the baths before absorption, i.e. the temperature of the medium surrounding the particle. This is different from pulsed experiments, in which the electron gas temperature can be orders thousands of K higher than room temperature.[48]

Radiative recombination gives rise to weakly emitting sources spectrally and spatially distributed throughout the particle over a broad frequency band with an exponential cutoff at $\hbar\omega_{\mathrm{L}} + k_{\mathrm{B}} T$. The weak recombination emission can be greatly enhanced by the surface plasmon resonance, acting as an antenna. Supplementary figure S1 shows a schematic representation of the described processes. With this model the following predictions can be made. Firstly the emission spectrum must follow the plasmon spectrum if the excitation laser is well above the plasmon resonance as shown in Figure 1. If the excitation falls within the plasmon resonance, the spectrum is expected to follow the plasmon spectrum multiplied by a Bose-Einstein statistics factor arising from phonon population (assuming phonon processes to dominate over carrier-carrier interactions). This factor should be proportional to $\bar{n}$ for anti-Stokes and $\bar{n} + 1$ for Stokes processes, where

$$\bar{n} = \left(\exp \frac{\hbar\omega}{k_B T} - 1 \right)^{-1}. \tag{1}$$

With this model, it can also be predicted that the emission should be polarized; for the longitudinal plasmon of gold nanorods this polarization coincides with the longitudinal axis of the particle.[37] Moreover, the lifetime should be determined by the lifetime of hot electrons and holes and should be significantly shorter than the thermalization time of the carriers. If this was not the case, a few interactions would be enough to reduce the carriers' energy and therefore the electron and hole wouldn't have enough energy to produce an optical photon.

Finally, only the presence of hot carriers is required in the model. One important assumption for this model is that the coupling mechanism of electron-hole pairs with the plasmons is flat within the plasmon energy band. Therefore excitation well above the plasmon resonance should excite the electron-hole pairs with nearly the same efficiency as just above the plasmon resonance.[23]

Here we propose to use the anti-Stokes luminescence emission from gold nanoparticles to determine their temperature. According to the model just described, the anti-Stokes emission follows the following form,

$$I(\omega) = \mathrm{I}_{\mathrm{SPR}}(\omega) \cdot \left(\exp \frac{\hbar(\omega - \omega_{\mathrm{L}})}{k_{\mathrm{B}} T} - 1 \right)^{-1} \tag{2}$$

where $I(\omega)$ is the emitted intensity, ω is the angular frequency of the photons, ω_{L} is the frequency of the laser, $\hbar$ is Planck's constant, k_{B} Boltzmann's constant. $\mathrm{I}_{\mathrm{SPR}}(\omega)$ is the surface plasmon resonance that can be obtained by exciting the particle at energies higher than the resonance. The only remaining free parameter is the temperature T (plus a normalization constant not included in eqn. 2.) This means that carefully fitting the emission spectra excited at two frequencies ($\nu \gg \nu_{\mathrm{SPR}}$ and $\nu \approx \nu_{\mathrm{SPR}}$) allows us to extract the absolute temperature of the particles without any previous calibration.

All the measurements in this work were performed with a home-built confocal microscope equipped a spectrometer (Acton 500i) in the emission path. We focused our lasers to a diffraction-limited spot using a $60X$, NA 1.4 oil immersion objective (Olympus) and collected the emitted photons through the same objective. This provided high excitation and collection efficiency. We employed a 532 nm (CNI) laser for characterizing the nanorods' plasmon and a 633 nm HeNe (Thorlabs) to excite the nanorods in resonance. We give more experimental details in the Supplementary Information.

Wet chemically synthesized nanorods[49] with average dimensions of 21 nm × 50 nm and a plasmon resonance around 650 nm were spin-coated onto clean coverslips, controlling the superficial concentration to obtain individual nanorods with the diffraction-limited optical

resolution. In addition, the samples were mounted in a flow cell that allowed us to increase the temperature of the medium up to 60 °C and to monitor it through a Pt100 resistance thermometer placed 1 mm away from the observation area. More details about the experimental setup are given in the Supplementary Information.

To compensate for the drift of the setup while increasing the temperature, we developed a computer program to continuously track a reference particle. The same program was responsible for recording the temperature and triggering the spectrometer. In this way complete data sets were acquired at different temperatures, including spectra while exciting at 532 nm, at 633 nm with different laser intensities and the temperature measured by the Pt100. A spectrum with 532 nm laser excitation was taken after every cycle to ensure that the particle under study had not reshaped due to higher excitation powers.

The intensity of the lasers was controlled via the voltage applied to an acousto-optic modulator in the optical path. Several accumulations of the spectra at the same laser intensity were recorded. This not only allowed us to lower the noise of the measurements because of a longer exposure time, but also allowed us to remove bright pixels generated by cosmic rays. Having several accumulations is also useful to monitor changes in the intensity of the spectra during the acquisition itself. These changes can be due to a drift of the setup while measuring or to a reshaping of the particle. If the reshaping was confirmed by comparing the spectra acquired with the 532 nm laser,[50] the measurements where rejected. If the changes in the observed emission spectra were due to drift of the setup, the particular data set was not taken into account. For the purposes of this work the excitation intensity is crucial for characterizing the method; if the particle is not in focus it would result in an overestimation of the excitation power.

The proposed model for the anti-Stokes emission requires to know the plasmon spectrum ($I_{SPR}(\omega)$ in equation 2) of the particle in order to fit the emission at shorter wavelengths and extract the particle temperature. It has been shown that both scattering and luminescence spectra roughly overlap over a broad range of wavelengths.[22] Therefore exciting gold

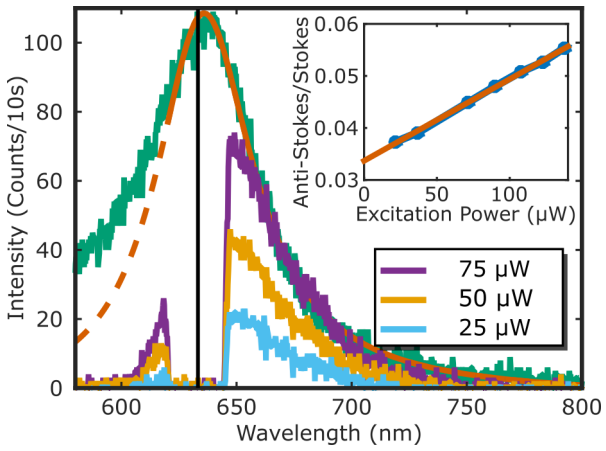

Figure 1: **Luminescence emission spectra of a single gold nanorod.** The green curve is the measured luminescence emission under 532 nm excitation with a Lorentzian fitting in red. The dashed part is the region that was not considered for the fitting. The other curves are the emission of the same particle under 633 nm irradiation at three different powers indicated in the legend. The inset shows the anti-Stokes-to-Stokes ratio as a function of the excitation power, overlapped with a linear fit in red. The dip centered on the laser wavelength is caused by the notch filter used to prevent the excitation laser from reaching the detectors.

nanorods with 532 nm allows us to record the longitudinal plasmon spectra, as shown in the green solid curve of Figure 1. The peak was fitted by a single Lorentzian, shown in red in the Figure; the dashed part of the curve is the spectral region that was not considered for the fitting. It has to be recalled that the luminescence spectrum is not a perfect Lorentzian since there is a broadband contribution to the luminescence arising between the excitation wavelength and the plasmon peak.[51] This appears as an asymmetry in the emission spectrum, particularly visible for wavelengths smaller than 625 nm. The results of this fitting will be employed for the I_{SPR} function defined in equation 2.

The other curves in Fig. 1 show the luminescence emission of the same nanorod while irradiating with a 633 nm laser at different powers, ranging from 25 μW to 75 μW at the back aperture of the objective. The vertical black line shows the wavelength of the laser. The Stokes part of the spectrum at longer wavelengths than the excitation shows the same shape as the plasmon emission observed under 532 nm excitation, apart from a normalization factor. From the figure it can readily be seen that the shape of the anti-Stokes emission,

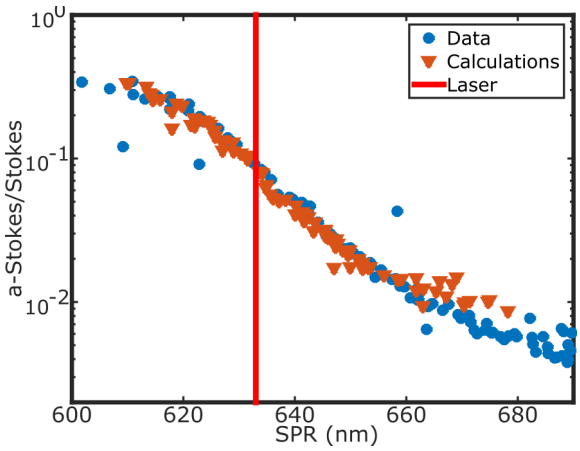

Figure 2: **Characterization of anti-Stokes emission for different SPR.** Ratio of the anti-Stokes to Stokes emission under 633 nm excitation as a function of the resonance wavelength of each particle. The blue circles are experimental results, while the red triangles are the results of the calculations with equation 1. There is a very good agreement between experiment and calculations. Particles with a resonance to the blue of the laser (indicated by the vertical red line) have an increased anti-Stokes emission.

at shorter wavelengths than excitation, is exponential-like and doesn't follow the Lorentzian shape of the Stokes emission. The dip between Stokes and anti-Stokes is caused by the notch filter that prevents direct excitation light from reaching the detectors.

The inset of Figure 1 shows the anti-Stokes-to-Stokes ratio of the integrated luminescence for different laser excitation intensities. It is possible to see that even with a linear behavior, the anti-Stokes intensity increases more rapidly with laser excitation power than the Stokes emission. We already exploited this phenomenon to image gold nanorods in high-background conditions.[38] Moreover it shows that the anti-Stokes emission depends on laser excitation power differently than its Stokes counterpart. For more information on the power dependence of both the anti-Stokes and Stokes luminescence, please refer to the Supplementary Information.

To further characterize this phenomenon, we measured the emission for 90 nanorods with different plasmon resonances under the same 633 nm excitation and calculated the ratio of integrated anti-Stokes to Stokes emission. Figure 2 shows the experimental results in blue circles, where the horizontal axis of the figure is the surface plasmon resonance (SPR) of each

particle. The vertical red line marks the laser wavelength. The particles shown in the plot had resonances between 600 nm and 690 nm; the ones showing the maximum ratio of anti-Stokes to Stokes are those with a resonance to the blue of the laser. For these particles the longitudinal plasmon is enhancing preferably the anti-Stokes emission. For particles with a resonance at the laser wavelength the anti-Stokes and the Stokes emission have similar enhancement and show a ratio close to 10%.

Figure 2 also shows the results of numerical calculations as the red triangles. An excellent overlap between the measured and the calculated data can be observed. The absorption cross section of several particles was calculated with the ADDA package.[14] Each calculated absorption spectrum was fitted by a Lorentzian and used as $I_{SPR}(\omega)$ in eqn. 2. Assuming a diffraction-limited laser spot and using the calculated absorption cross section allowed us to calculate the temperature of the particle. This value was used in eqn. 2 to compute the anti-Stokes emission spectrum. The Stokes emission was set proportional to the excitation power with a shape given by the calculated absorption spectra. Since both anti-Stokes and Stokes emissions are proportional to the excitation power, this term cancels out when computing the ratio. The laser power therefore only enters into the equation when calculating the temperature of the particles. It is remarkable that the agreement between data and calculations was achieved without free parameters, solely taking into account the transmission spectra of the filters.

Furthermore, by fitting the anti-Stokes part of the spectra shown in Figure 1 with equation 2 it is possible to extract the temperature of the particle at each excitation power. Figure 3 shows the results of this procedure. The spectra shown were recorded at 4 different excitation intensities while the full lines are the fits; again, there is an excellent agreement between data and model. For every anti-Stokes measurement we have also acquired the full plasmon spectrum while exciting with a 532 nm laser before and after the temperature extraction. The full plasmon spectrum is necessary to calculate the parameters of $I_{SPR}(\omega)$ from equation 2 and also to verify that the particle did not reshape while being excited at

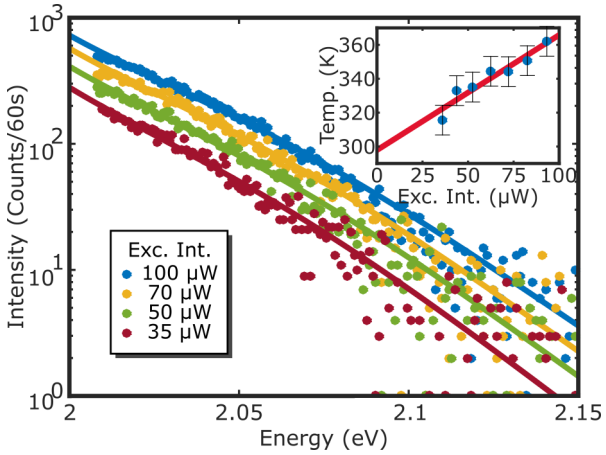

Figure 3: **Anti-Stokes emission at different irradiation powers.** We used the model from equation 2 to fit the experimental data. There is an excellent agreement between data and model. The inset shows the extracted temperature at each power (blue dots) and a linear extrapolation of the data to $0\,\mu$W excitation power. The value obtained for room temperature was 293 K while the measured value was 296 K.

resonance.

The inset in Figure 3 shows the temperatures resulting from the fits at different irradiation intensities (blue dots). It has to be noted that the absolute temperatures of the particle at each excitation power were calculated without any calibration. As expected, the temperature of the nanorod is proportional to the excitation intensity, or equivalently to the absorbed energy. Thus, this method provides an *in situ* way to measure the temperature reached by nanoparticles when they are excited with resonant monochromatic light. Additionally, from these data sets it is also possible to calculate the temperature at $0\,\mu$W excitation power, i.e. room temperature, by extrapolating the results with a linear fit. The value we obtained in this case is 293 ± 6 K, while room temperature was 296 K, a 2% accuracy.

The accuracy of the obtained temperature depends to a great extent on the plasmon resonance. The first step in the fitting procedure is the determination of the term $I_{\mathrm{SPR}}(\omega)$ in equation 2. This is achieved by fitting a Lorentzian to the emission spectrum obtained while irradiating with a 532 nm laser. In figure 1 it is possible to observe that the emission spectrum is not perfectly Lorentzian and therefore the fitting results will be sensitive to the portion of the spectrum selected. Depending on the wavelength range selected, the

parameters of the Lorentzian fit (its width and peak position) can slightly change therefore giving rise to different temperatures when fitting the anti-Stokes emission spectrum.

Equation 2 shows that when the resonance is to the red of the laser, the term $I_{\mathrm{SPR}}(\omega)$ will slowly vary in the region where the anti-Stokes emission is observed. Therefore small changes in the parameters of the Lorentzian fit will have a small effect on the temperature extracted. However, particles that are not in resonance with the excitation laser will present a lower emission due to a smaller absorption cross section and to a lower enhancement of the anti-Stokes emission (see for example figure 2). The error bar in figure 3 and in the following figures is the result of the estimation of the temperature uncertainty because of variations in the plasmon resonance fit.

As expected from the model, the anti-Stokes emission should depend not only on the particle's intrinsic properties but also on the temperature of the surrounding medium. [52] In order to test this point, we changed the temperature of the sample in a controlled manner and recorded the luminescence emitted by a single nanorod.

For this set of experiments we employed an air objective ($60X$, NA 0.9, Olympus) to avoid the presence of a heat sink directly in contact with the observed area. We employed higher laser powers to compensate for the lower excitation efficiency. At each temperature several spectra were acquired at different 633 nm excitation powers and also a spectrum of the plasmon before and after each measurement in order to monitor any possible reshaping of the particles during the experiment.

Figure 4 shows the extracted temperature of a particle at varying excitation powers and at different water temperatures. The blue squares are the results of the measurement at 20 ^{o}C, while the green crosses are measured at 40 ^{o}C and the yellow circles at 60 ^{o}C. The full lines are the calculated temperatures for a particle with plasmon overlapping the measured one and assuming a diffraction-limited focus spot. For the dimensions of the particle, the mean values from TEM images were used and the length was adjusted to obtain the measured resonance. There is a remarkable agreement between the calculation and the measured

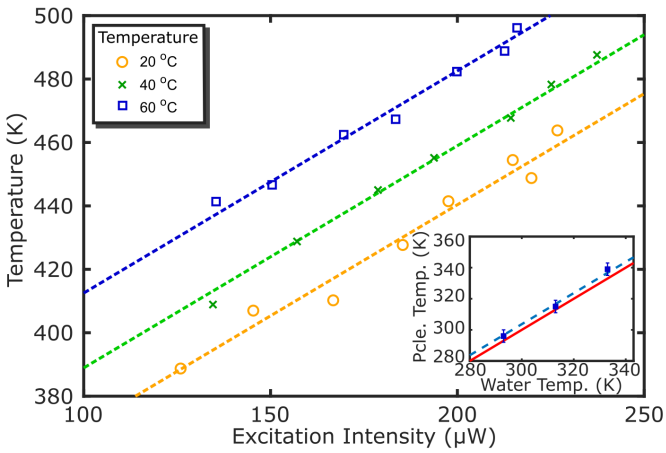

Figure 4: **Calibration-free temperature measurement.** Anti-Stokes-luminescence extracted temperatures for an individual nanorod at different excitation powers and at different sample temperatures. The dashed lines lines are fits with the same slope for the three temperatures. The circles in the inset plot show the local temperature of the sample obtained by extrapolating temperature at zero excitation power as a function of the water temperature. The red line represents the expected curve if both temperatures are identical (equal). The dashed blue line is a fit to the data points with unit slope that shows a systematic offset of 3.8 K, a %1.2 difference.

values. Moreover it is possible to extrapolate the temperature at zero excitation power for each case as was explained earlier. The results are shown in the inset of the figure for each temperature. The red line with slope 1 is a guide to the eye.

Figure 4 clearly shows that the extracted temperature varies with the temperature of the surrounding medium. More strikingly the method does not require any previous calibration nor adjustment. The values obtained with the extrapolation to 0 μW excitation power were 296 ± 4 K, 315 ± 4 K and 339 ± 4 K for water temperatures of 293 K, 313 K and 333 K respectively. The inset plot in figure 4 presents these points and a red solid line with the expected curve if both temperatures are identical. The dashed line shows a fit of the data that evidences a small systematic offset of 3.8 K. This represents an inaccuracy of %1.2 which is a good result for a calibration-free method. Notably, the presented calibration-free procedure would allow us to perform the same measurements in any other setup and could act as a reference for calibration of other nano thermometers.

Being able to control and monitor temperature at the nanoscale is of utmost importance

in different fields ranging from photothermal therapy[5] to nano fabrication.[53] In this work we have shown a simple procedure that allows us to measure the temperature of single gold nanorods irradiated by a monochromatic continuous laser and without any previous calibration. The level of accuracy of the temperature measurement depends on several factors, but for nanorods it can be estimated to be better than 6 K.

The model employed for describing the anti-Stokes emission takes into account the plasmon, responsible for enhancing the emission, as well the electron-hole pairs interaction with the thermal baths, where coupling to phonons is the dominant process. It has been shown that the correct characterization of the plasmonic resonance is fundamental for the proper extraction of temperature, specially in cases where the resonance is to the blue of the excitation wavelength.

Particles with a resonance to the red of the excitation wavelength would be more reliable in the temperature extraction procedure, but would also exhibit a lower emission towards shorter wavelengths. The trade-off between both effects and the possibility to fully characterize the plasmon resonance, will determine the specific particles that are better suited for each application.

A possible improvement for this technique would be the use nanostructures with a narrow shape distribution such as gold bipyramids.[54] Such structures would be ideal candidates for temperature extraction since they present negligible size dispersion and thus their plasmon can be measured in bulk or determined from theory, avoiding the need of a second excitation source. This would reduce the main source of inaccuracies for the method.

The proposed method doesn't require any calibration, since the only free parameter of the model is the absolute temperature of the nanoparticle under study. Moreover the recording of the anti-Stokes spectrum is readily achievable in any confocal microscope with a coupled spectrometer. A 6 K accuracy may suffice for several applications; it is important to point out that this value can be improved in different ways: by carefully selecting the particles that show the most favorable plasmon resonance; by determining the plasmon resonance through

white-light scattering, avoiding the uncertainty in the fit; by increasing the exposure times to increase the signal-to-noise ratio.

Acknowledgement

This work has been financed by FOM, which is part of the Netherlands Organisation for Scientific Research (NWO) (programme number 11SGC02) and by NWO (grant ECHO 712.013.003).

Supporting Information Available

Scheme for the Au NR luminescence mechanism. Details concerning the experimental setup. Luminescence power dependence. Gold Nanorod temperature calculations.

References

(1) Yang, J.-M.; Yang, H.; Lin, L. Quantum Dot Nano Thermometers Reveal Heterogeneous Local Thermogenesis in Living Cells. *ACS Nano* **2011**, *5*, 5067–5071.

(2) Hrelescu, C.; Stehr, J.; Ringler, M.; Sperling, R. A.; Parak, W. J.; Klar, T. A.; Feldmann, J. DNA Melting in Gold Nanostove Clusters. *J. Phys. Chem. C* **2010**, *114*, 7401–7411.

(3) Li, Y.; Gobin, A. M.; Dryden, G. W.; Kang, X.; Xiao, D.; Li, S. P.; Zhang, G.; Martin, R. C. G. Infrared light-absorbing gold/gold sulfide nanoparticles induce cell death in esophageal adenocarcinoma. *Int. J. Nanomedicine* **2013**, *8*, 2153–2161.

(4) Gobin, A. M.; Lee, M. H.; Halas, N. J.; James, W. D.; Drezek, R. A.; West, J. L. Near-Infrared Resonant Nanoshells for Combined Optical Imaging and Photothermal Cancer Therapy. *Nano Lett.* **2007**, *7*, 1929–1934.

(5) Huang, X. H.; El-Sayed, I. H.; Qian, W.; El-Sayed, M. a. Cancer cell imaging and photothermal therapy in the near-infrared region by using gold nanorods. *J. Am. Chem. Soc.* **2006**, *128*, 2115–2120.

(6) Huo, S.; Jin, S.; Ma, X.; Xue, X.; Yang, K.; Kumar, A.; Wang, P. C.; Zhang, J.; Hu, Z.; Liang, X.-J. Ultrasmall Gold Nanoparticles as Carriers for Nucleus-Based Gene Therapy Due to Size-Dependent Nuclear Entry. *ACS Nano* **2014**, *8*, 5852–5862.

(7) Ebrahimi, S.; Akhlaghi, Y.; Kompany-Zareh, M.; Rinnan, A. Nucleic Acid Based Fluorescent Nanothermometers. *ACS Nano* **2014**,

(8) Liu, X.; Siegler, M. A.; Bouwman, E. Ratiometric Thermometer Based on a Lanthanoid Coordination Polymer. *European Journal of Inorganic Chemistry* **2016**, *2016*, 2984–2988.

(9) Vetrone, F.; Naccache, R.; Zamarrón, A.; Juarranz de la Fuente, A.; Sanz-Rodríguez, F.; Martinez Maestro, L.; Martín Rodriguez, E.; Jaque, D.; García Solé, J.; Capobianco, J. A. Temperature sensing using fluorescent nanothermometers. *ACS Nano* **2010**, *4*, 3254–8.

(10) Pozzi, E. A.; Zrimsek, A. B.; Lethiec, C. M.; Schatz, G. C.; Hersam, M. C.; Van Duyne, R. P. Evaluating Single-Molecule Stokes and Anti-Stokes SERS for Nanoscale Thermometry. *J. Phys. Chem. C* **2015**, *119*, 21116–21124.

(11) Zijlstra, P.; Orrit, M. Single metal nanoparticles: optical detection, spectroscopy and applications. *Reports Prog. Phys.* **2011**, *74*, 106401.

(12) Carattino, A.; Khatua, S.; Orrit, M. In situ tuning of gold nanorod plasmon through oxidative cyanide etching. *Phys. Chem. Chem. Phys.* **2016**, *18*, 15619–15624.

(13) Draine, B. T.; Flatau, P. J. Discrete-Dipole Approximation For Scattering Calculations. *J. Opt. Soc. Am. A* **1994**, *11*, 1491.

(14) Yurkin, M. A.; Hoekstra, A. G. The discrete-dipole-approximation code ADDA: Capabilities and known limitations. *J. Quant. Spectrosc. Radiat. Transf.* **2011**, *112*, 2234–2247.

(15) Oskooi, A. F.; Roundy, D.; Ibanescu, M.; Bermel, P.; Joannopoulos, J.; Johnson, S. G. Meep: A flexible free-software package for electromagnetic simulations by the FDTD method. *Comput. Phys. Commun.* **2010**, *181*, 687–702.

(16) Hu, M.; Novo, C.; Funston, A.; Wang, H.; Staleva, H.; Zou, S.; Mulvaney, P.; Xia, Y.; Hartland, G. V. Dark-field microscopy studies of single metal nanoparticles: understanding the factors that influence the linewidth of the localized surface plasmon resonance. *J. Mater. Chem.* **2008**, *18*, 1949.

(17) Boyer, D.; Tamarat, P.; Maali, A.; Lounis, B.; Orrit, M. Photothermal imaging of nanometer-sized metal particles among scatterers. *Science* **2002**, *297*, 1160–1163.

(18) Berciaud, S.; Lasne, D.; Blab, G.; Cognet, L.; Lounis, B. Photothermal heterodyne imaging of individual metallic nanoparticles: Theory versus experiment. *Phys. Rev. B* **2006**, *73*, 045424.

(19) Tcherniak, A.; Dominguez-Medina, S.; Chang, W. S.; Swanglap, P.; Slaughter, L. S.; Landes, C. F.; Link, S. One-photon plasmon luminescence and its application to correlation spectroscopy as a probe for rotational and translational dynamics of gold nanorods. *J. Phys. Chem. C* **2011**, *115*, 15938–15949.

(20) Fang, Y.; Chang, W.-S.; Willingham, B.; Swanglap, P.; Dominguez-Medina, S.; Link, S. Plasmon emission quantum yield of single gold nanorods as a function of aspect ratio. *ACS Nano* **2012**, *6*, 7177–84.

(21) Rao, W.; Li, Q.; Wang, Y.; Li, T.; Wu, L. Comparison of Photoluminescence Quantum Yield of Single Gold Nanobipyramids and Gold Nanorods. *ACS Nano* **2015**, *9*, 2783–2791.

(22) Yorulmaz, M.; Khatua, S.; Zijlstra, P.; Gaiduk, A.; Orrit, M. Luminescence quantum yield of single gold nanorods. *Nano Lett.* **2012**, *12*, 4385–91.

(23) Cheng, Y.; Lu, G.; He, Y.; Shen, H.; Zhao, J.; Xia, K.; Gong, Q. Luminescence Quantum Yields of Gold Nanoparticles Varying with Excitation Wavelength. *Nanoscale* **2015**, 2188–2194.

(24) Wang, H.; Huff, T. B.; Zweifel, D. A.; He, W.; Low, P. S.; Wei, A.; Cheng, J.-X. In vitro and in vivo two-photon luminescence imaging of single gold nanorods. *Proc. Natl. Acad. Sci.* **2005**, *102*, 15752–15756.

(25) Huang, X.; Jain, P. K.; El-Sayed, I. H.; El-Sayed, M. A. Plasmonic photothermal therapy (PPTT) using gold nanoparticles. *Lasers Med. Sci.* **2008**, *23*, 217–228.

(26) Kang, B.; Afifi, M. M.; Austin, L. a.; El-Sayed, M. a. Exploiting the nanoparticle plasmon effect: observing drug delivery dynamics in single cells via Raman/fluorescence imaging spectroscopy. *ACS Nano* **2013**, *7*, 7420–7.

(27) Hirsch, L. R.; Stafford, R. J.; Bankson, J. A.; Sershen, S. R.; Rivera, B.; Price, R. E.; Hazle, J. D.; Halas, N. J.; West, J. L. Nanoshell-mediated near-infrared thermal therapy of tumors under magnetic resonance guidance. *Proc. Natl. Acad. Sci. U. S. A.* **2003**, *100*, 13549–54.

(28) O'Neal, D.; Hirsch, L. R.; Halas, N. J.; Payne, J.; West, J. L. Photo-thermal tumor ablation in mice using near infrared-absorbing nanoparticles. *Cancer Lett.* **2004**, *209*, 171–176.

(29) Zhao, T.; Yu, K.; Li, L.; Zhang, T.; Guan, Z.; Gao, N.; Yuan, P.; Li, S.; Yao, S. Q.; Xu, Q.-H.; Xu, G. Q. Gold Nanorod Enhanced Two-Photon Excitation Fluorescence of Photosensitizers for Two-Photon Imaging and Photodynamic Therapy. *ACS Appl. Mater. Interfaces* **2014**, *6*, 2700–2708.

(30) Donner, J. S.; Thompson, S. a.; Alonso-Ortega, C.; Morales, J.; Rico, L. G.; Santos, S. I. C. O.; Quidant, R. Imaging of Plasmonic Heating in a Living Organism. *ACS Nano* **2013**, *7*, 8666–8672.

(31) Mooradian, A. Photoluminescence of metals. *Phys. Rev. Lett.* **1969**, *22*, 185–187.

(32) Mohamed, M. B.; Volkov, V.; Link, S.; El-Sayed, M. A. The 'lightning' gold nanorods: fluorescence enhancement of over a million compared to the gold metal. *Chem. Phys. Lett.* **2000**, *317*, 517–523.

(33) Beversluis, M.; Bouhelier, A.; Novotny, L. Continuum generation from single gold nanostructures through near-field mediated intraband transitions. *Phys. Rev. B* **2003**, *68*, 1–10.

(34) Dulkeith, E.; Niedereichholz, T.; Klar, T.; Feldmann, J.; von Plessen, G.; Gittins, D.; Mayya, K.; Caruso, F. Plasmon emission in photoexcited gold nanoparticles. *Phys. Rev. B* **2004**, *70*, 205424.

(35) Link, S.; El-Sayed, M. A. Shape and size dependence of radiative, non-radiative and photothermal properties of gold nanocrystals. *Int. Rev. Phys. Chem.* **2000**, *19*, 409–453.

(36) Jiang, L.; Schie, I. W.; Qian, J.; He, S.; Huser, T. Coherent Anti-Stokes Emission from Gold Nanorods and its Potential for Imaging Applications. *ChemPhysChem* **2013**, *14*, 1951–1955.

(37) He, Y.; Xia, K.; Lu, G.; Shen, H.; Cheng, Y.; Liu, Y.-c.; Shi, K.; Xiao, Y.-F.; Gong, Q. Surface enhanced anti-Stokes one-photon luminescence from single gold nanorods. *Nanoscale* **2015**, *7*, 577–582.

(38) Carattino, A.; Keizer, V. I.; Schaaf, M. J.; Orrit, M. Background suppression in imaging gold nanorods through detection of anti-stokes emission. *Biophysical journal* **2016**, *111*, 2492–2499.

(39) Hodak, J. H.; Henglein, A.; Hartland, G. V. Electron-phonon coupling dynamics in very small (between 2 and 8 nm diameter) Au nanoparticles. *J. Chem. Phys.* **2000**, *112*, 5942–5947.

(40) Giri, A.; Gaskins, J. T.; Foley, B. M.; Cheaito, R.; Hopkins, P. E. Experimental evidence of excited electron number density and temperature effects on electron-phonon coupling in gold films. *J. Appl. Phys.* **2015**, *117*, 044305.

(41) Arbouet, A.; Voisin, C.; Christofilos, D.; Langot, P.; Fatti, N. D.; Vallée, F.; Lermé, J.; Celep, G.; Cottancin, E.; Gaudry, M.; Pellarin, M.; Broyer, M.; Maillard, M.; Pileni, M. P.; Treguer, M. Electron-Phonon Scattering in Metal Clusters. *Phys. Rev. Lett.* **2003**, *90*, 177401.

(42) Huang, J.; Wang, W.; Murphy, C. J.; Cahill, D. G. Resonant secondary light emission from plasmonic Au nanostructures at high electron temperatures created by pulsed-laser excitation. *Proc. Natl. Acad. Sci. U. S. A.* **2014**, *111*, 906–11.

(43) Sönnichsen, C.; Franzl, T.; Wilk, T.; von Plessen, G.; Feldmann, J.; Wilson, O.; Mulvaney, P. Drastic Reduction of Plasmon Damping in Gold Nanorods. *Phys. Rev. Lett.* **2002**, *88*, 077402.

(44) Sundararaman, R.; Narang, P.; Jermyn, A. S.; Goddard III, W. A.; Atwater, H. A. Theoretical predictions for hot-carrier generation from surface plasmon decay. *Nature communications* **2014**, *5*.

(45) Brongersma, M. L.; Halas, N. J.; Nordlander, P. Plasmon-induced hot carrier science and technology. *Nat. Nanotechnol.* **2015**, *10*, 25–34.

(46) Manjavacas, A.; Liu, J. G.; Kulkarni, V.; Nordlander, P. Plasmon-Induced Hot Carriers in Metallic Nanoparticles. *ACS Nano* **2014**, *8*, 7630–7638.

(47) Pustovalov, V. K. Theoretical study of heating of spherical nanoparticle in media by short laser pulses. *Chem. Phys.* **2005**, *308*, 103–108.

(48) Baffou, G.; Berto, P.; Bermúdez Ureña, E.; Quidant, R.; Monneret, S.; Polleux, J.; Rigneault, H. Photoinduced Heating of Nanoparticle Arrays. *ACS Nano* **2013**, *7*, 6478–6488.

(49) Nikoobakht, B.; El-Sayed, M. A. Preparation and Growth Mechanism of Gold Nanorods (NRs) Using Seed-Mediated Growth Method. *Chem. Mater.* **2003**, *15*, 1957–1962.

(50) Liu, Y.; Mills, E. N.; Composto, R. J. Tuning optical properties of gold nanorods in polymer films through thermal reshaping. *J. Mater. Chem.* **2009**, *19*, 2704.

(51) Boyd, G. T.; Yu, Z. H.; Shen, Y. R. Photoinduced luminescence from the noble metals and its enhancement on roughened surfaces. *Phys. Rev. B* **1986**, *33*, 7923–7936.

(52) Konrad, A.; Wackenhut, F.; Hussels, M.; Meixner, A. J.; Brecht, M. Temperature Dependent Luminescence and Dephasing of Gold Nanorods. *J. Phys. Chem. C* **2013**, *117*, 21476–21482.

(53) Fedoruk, M.; Meixner, M.; Carretero-Palacios, S.; Lohmuller, T.; Feldmann, J. Nanolithography by Plasmonic Heating and Optical Manipulation of Gold Nanoparticles. *ACS Nano* **2013**, *7*, 7648–7653.

(54) Pelton, M.; Sader, J. E.; Burgin, J.; Liu, M.; Guyot-Sionnest, P.; Gosztola, D. Damping of acoustic vibrations in gold nanoparticles. *Nat. Nanotechnol.* **2009**, *4*, 492–495.